Supporting Information: Long-range dipole-dipole interactions in a plasmonic lattice

Ashwin K. Boddeti,[†] Jun Guan,[‡] Tyler Sentz,[†] Xitlali Juarez,[¶] Ward Newman,[§] Cristian Cortes,[‖] Teri W. Odom,[⊥] and Zubin Jacob[*,†]

[†]*Elmore Family School of Electrical and Computer Engineering, Birck Nanotechnology Center, Purdue University, West Lafayette, Indiana 47907, USA*

[‡]*Department of Chemistry, Northwestern University, Evanston, Illinois 60208, USA*

[¶]*Department of Materials Science and Engineering, Northwestern University, Evanston, Illinois 60208, USA*

[§] *Intel Corporation, Hillsboro, Oregon 97124, USA*

[‖]*Center for Nanoscale Materials, Argonne National Laboratory, Lemont, Illinois 60439, USA*

[⊥] *Department of Chemistry, and Department of Materials Science and Engineering, Northwestern University, Evanston, Illinois 60208, USA*

E-mail: zjacob@purdue.edu

In this supporting information, we discuss how we compute the angle-resolve extinction spectra, calculate the normalized energy transfer rate using the dyadic Green's function, discuss the experimental setup, sample fabrication process, estimation of the polymer thinfilm thickness, mean nearest-neighbour separation between the donor-acceptor pairs, the physical origin of persistant DDI interactions at low densities, and the statistics on spread of mean

decay rate values at high dilution factors.

Numerical Simulations

Angle-resolved Extinction

Angle resolve extinction is numerically calculated using FDTD simulations.[1] The transmission spectra for a single Ag nano-pillar with Bloch periodic boundary conditions in the plane of the structure and perfectly matched layers (PML) in the direction normal to the structure are used. A plane wave source is placed within the glass substrate. The incident angle of the plane wave source is swept by changing the angle of the plane wave. The transmission, T is measured at each angle and subsequently the extinction is calculated as E = 1-T. The $k_{||}$ wave-vector is related to the angle of incidence through the relation, $k_{||} = nk_0 sin(\theta) = n\frac{2\pi}{\lambda} sin(\theta)$, where λ is the wavelength, n is the index of the substrate. A uniform index environment is necessary to excite the collective lattice mode, this is incorporated in to the FDTD simulations by changing the background index.

Computing the dyadic Green's function

The dyadic Green's function $\overline{\overline{\mathbf{G}}}$, is defined by the electric field at a position $\mathbf{r_A}$ generated by a point source at position $\mathbf{r_D}$ with dipole moment μ,[2]

$$\mathbf{E}(\mathbf{r_A}) = \frac{\omega^2}{\epsilon_0 \epsilon_r c^2} \overline{\overline{\mathbf{G}}}(\mathbf{r_A}, \mathbf{r_D}).\mu \tag{1}$$

Each component of $\overline{\overline{\mathbf{G}}}$ is calculated using the corresponding orientation of the dipole and electric field component as

$$G_{xx} = \frac{\epsilon_0 \epsilon_r c^2}{\mu \omega^2} E_{xx} \tag{2}$$

The off-diagonal elements are found by taking the corresponding electric field components for a given orientation of the electric dipole. The dimensionless energy transfer rate is calculated using

$$\frac{\Gamma_{ET}}{\gamma_0} = 18\pi f(\omega_D)\sigma_a(\omega_D)|\mathbf{n_A}.\overline{\overline{\mathbf{G}}}(\mathbf{r_A}, \mathbf{r_D}; \omega_\mathbf{D}).\mathbf{n_D}|^2 \tag{3}$$

where $f(\omega_D)$ is the fluorescence emission of donor molecules, σ_A is the absorption cross-section of the acceptor molecules, $\mathbf{n_A}$, and, $\mathbf{n_D}$ are the unit vectors corresponding to the donor dipole and acceptor dipole orientations. Using FDTD simulations, the electric field due a point dipole placed on top of the structure is estimated. Subsequently, the components of the dyadic Green's function are estimated by running the simulation with test dipole oriented along x-,y-,z-directions. A $2\mu m \times 2\mu m$ structure is simulated with perfectly-matched-layer (PML) boundaries. A uniform index environment is necessary to excite the collective lattice mode, this is incorporated in to the FDTD simulations by changing the background index.

Experimental Setup

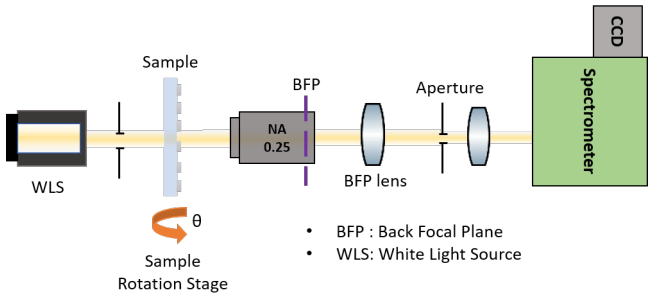

Figure 1: The schematic shows the experimental setup used in the angle-resolved transmission measurements.

Angle resolved extinction measurements are performed to map the dispersive modes supported by the nanophotonic structure. To this end, angle-resolved transmission spectra $T = I_{lattice}/I_{reference}$ are measured by focusing the back focal plane of the objective to the slit of the spectrometer (Acton SpectraPro SP-2300). An unpolarized laser-driven broadband white light source (Energetiq LDLS EQ-99x) is used in the measurements, see Fig.1. To

provide a homogeneous refractive index environment, the plasmonic lattice is embedded in an index matching fluid (n = 1.52) and covered with a borosillicate cover slip (superstrate). The extinction spectra are obtained as $E = 1 - T$ and is subsequently used to find the dispersion of the lattice. We have assumed th reflection from the silver nanoparticles to be small and neglegible in the extinction calculation. This assumption leads to a slight over-estimation in the extinction spectrum values. We quantify this deviation by comparing the measured

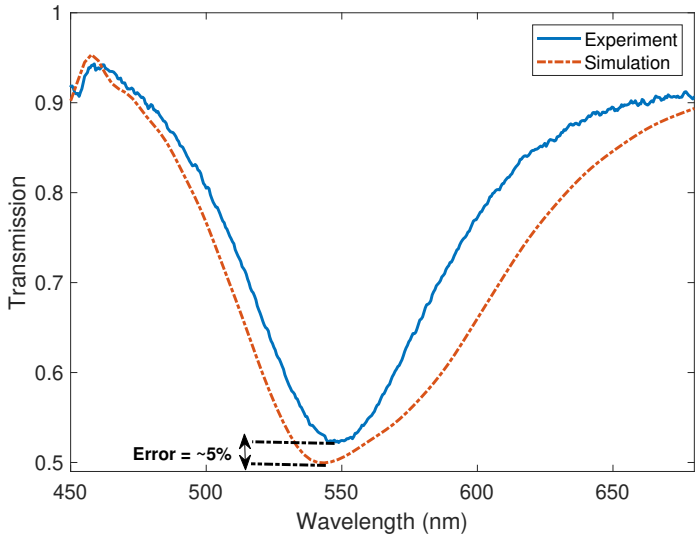

Figure 2: Comparison between the measured and calculated transmission spectra at normal incidence, i.e., $k_{||} = 0$.

extinction spectrum to that calculated using FDTD simulations. The deviation between the experimentally measured transmission spectrum and simulated transmission spectrum is $\sim 5\%$ at normal incidence, i.e, $k_{||} = 0$ as shown in the Fig. 2. We also note that the resonance dip in the transmission spectrum varies by $\sim$5 nm between the experiment and simulation. The good correspondence between the measured spectra and the FDTD simulation spectra confirm that neglecting the reflection from the nanoparticles is a reasonable assumption. This only leads to a slight deviation ($\sim 5\%$) in the extinction value (E = 1-T). Furthermore, considering the reflection spectra contribution would yield qualitatively similar results and does not effect the qualitative understanding of the results.

The spectrum and lifetimes are measured using the experimental setup shown in Fig.3.

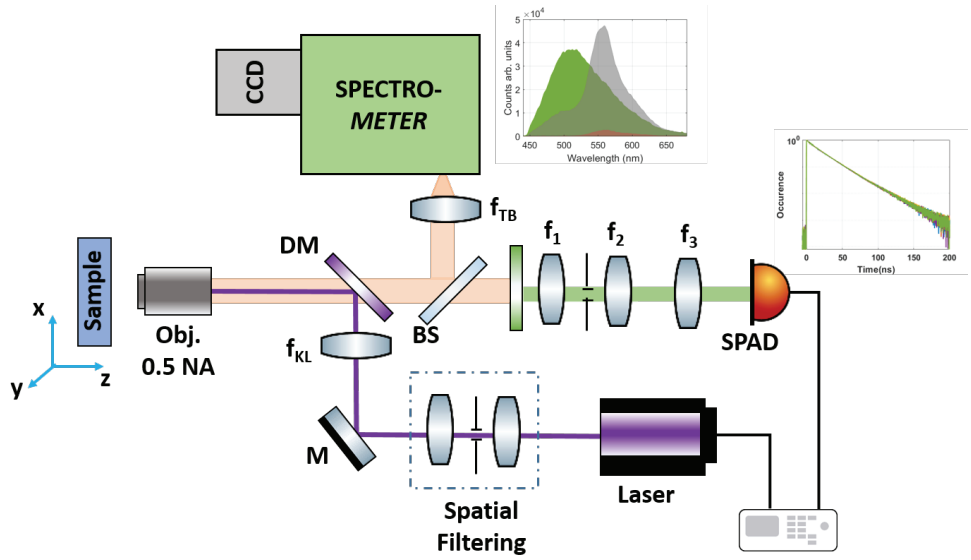

Figure 3: The schematic shows the experimental setup used for lifetime and spectral measurements. DM: Dichroic mirror, M: Mirror, f_{KL}: Köhler illumination lens, f_{TB}: tube lens, f_1, f_2 and f_3 are achromatic lenses.

The dye molecules are confocally excited using a ∼23 ps at 405 nm pulsed laser (Alphalas Picopower-LD-405). A Köhler illumination lens (f_{KL}) is used behind the objective (NA = 0.5) to ensure uniform illumination and prevent photo-bleaching of the donor (Alq_3) dye molecules. The collected fluorescence is used for measuring the spectrum and the decay traces. A narrowband filter (520 ± 5 nm) is used to collect photons at the peak emission wavelength of donors. The decay trace are recorded using the principles of time-correlated single photon counting (TCSPC). A single photon avalanche diode (MPD PDM series) is

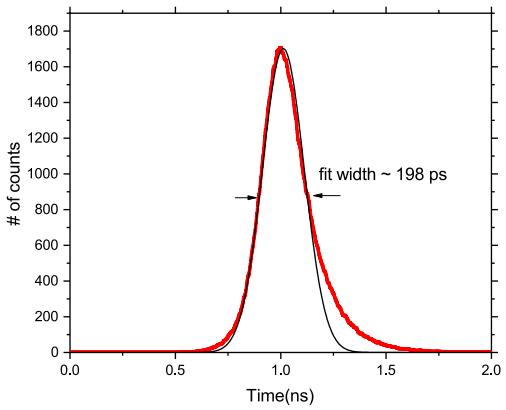

Figure 4: The instrument response function of the TCSPC setup.

used in conjunction with photon arrival counter board (PicoQuant HydraHarp 400) to detect and time tag the arrival time of the photons after laser excitation pulse (pulsewidth ∼23 ps). The fluorescence lifetime decay trace is found by binning the detected single photons based on their arrival time after the excitation pulse. Figure4 shows the instrument response function (IRF) of the TCSPC set-up used in the lifetime measurements. The IRF is recorded by detecting the reflection of the laser excitation pulses from a glass substrate. A Gaussian function fit estimates the IRF to be ∼198 ps FWHM. The measured IRF results from the convolution of the response functions of the SPAD, specified to be ∼35 ps FWHM by the manufacturer, of the acquisition system (electronics) and of the laser pulse duration.

Sample Fabrication

The silver (Ag) plasmonic lattice on fused silica is fabricated with a soft nanofabrication process. First, periodic photoresist posts on Si wafers are generated by solvent-assisted nanoscale embossing ($SANE$[35]). After Cr deposition (8 nm) followed by liftoff of photoresist posts, Si etching (300 nm), and gold (Au) deposition (80 nm), Au nanohole films are produced on the Si substrate with a Cr adhesion layer in between. The Au nanohole film is released from Si wafer by wet etching the Cr layer. The Au film is then floated on water and transferred to a fused silica substrate. A 2 nm thick Cr is deposited followed by 75 nm Ag through the Au hole film. The Au hole film is removed with tape and Ag nano-particle lattice is patterned on the silica substrate. The 2 nm Cr layer is used to improve adhesion between Ag NPs and silica. A 5 nm Al_2O_3 layer is deposited on top of Ag nano-particle lattice to prevent oxidation and sulfidation of Ag. Figure 5 shows the scanning Atomic force microscope image of the fabricated structures.

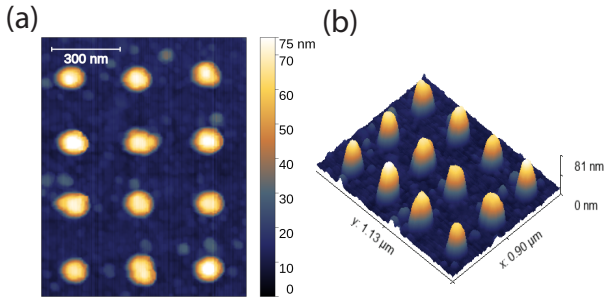

Figure 5: Scanning Atomic Force Microscope image of the sample.

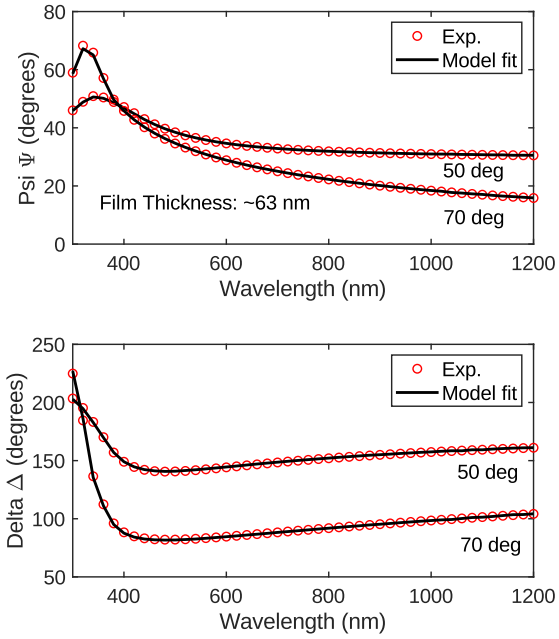

Figure 6: Spectroscopic ellipsometry measurements and modeling for the thinfilm thickness. The measurement provide estimates of the thickness of the thinfim to be ∼63 nm ± 2 nm.

Polymer thinfilm thickness

The dye molecule solutions are prepared in chloroform ($CHCl_3$). This solution is then mixed in a neutral solution consisting of Poly-methyl methacrylate (PMMA), Zeon Electron beam Positive-tone resist (ZEP-A) and choloroform ($CHCl_3$) in 2:2:1 ratio to form the stock solutions. These stock solutions have a donor dye number densities of $\sim 5.14 \times 10^{23}$ molecules/m^3 and acceptor dye number densities of $\sim 1.5 \times 10^{23}$ molecules/m^3 respectively. The polymer thinfilms are made by spin coating the stock solution on to the sample. The

samples are cured at 90^o C to evaporate any reminiscent volatile solvents left during the spin coating process. The curing leads to the formation of solid polymer thin-films with the dye molecules embedded in them. The typical thickness of the polymer thin-films is estimated to be $\sim$63 nm $\pm$ 2 nm using broadband visible ellipsometry measurements shown in Fig. 6. Subsequent lower acceptor concentration solutions are prepared by diluting the stock solution with the neutral solution.

Mean nearest-neighbour separation between donor-acceptor pairs

In order to study the dependence of dipole-dipole interaction strength on the separation between the donor and acceptor molecules the lifetime measurements are performed across various concentrations of acceptor molecules whilst keeping the donor concentration fixed. Statistically in the donor-acceptor binary mixture, varying the concentration of the acceptors changes the mean nearest-neighbour (N-N) separation between the donor-acceptor pairs in the ensemble. We estimate this mean nearest-neighbour separation using the probability distribution function for a binary mixture with finite sized particles.[3] Figure 7 shows the estimated mean nearest-neighbour distance between a donor-acceptor molecules pair. A fixed donor concentration ensures that the strength of the dispersive electromagnetic modes that mediate the interaction remain the same across various mean separation distances between donor-acceptor molecule pairs. This enables one to extract ensemble averaged dipole-dipole interaction strength at various mean separation distances between the donors and acceptors. Since we are dealing with a binary mixture consisting of donor and acceptor molecules, the nearest-neighbour distribution function $H(r)$ is associated with the probability of finding a nearest acceptor molecules at a distance r from a reference donor molecule. The probability

distribution function is given as,[3]

$$H(r) = \begin{cases} 0, & x < 1 \\ \frac{1}{\sigma}\frac{4\eta(2\frac{r}{\sigma}-\eta)}{(1-\eta)^2} exp\left(\frac{-4\eta}{(1-\eta)^2}[((\frac{r}{\sigma})^2-1)+\eta(\frac{r}{\sigma}-1)]\right) & x > 1 \end{cases} \tag{4}$$

where, $x = r/\sigma$ is the scaled distance, σ is the diameter of the donor molecule (~ 0.8 nm), $\eta = \rho\pi r^2(\sigma/2)$ is the reduced number density of the acceptor molecules and ρ is number density of acceptor molecules per unit area. The mean nearest-neighbour separation is found by using the first moment of the probability distribution function, $H(r)$,

$$\langle r \rangle = \int rH(r)dr \tag{5}$$

In order to get an estimate of the mean nearest-neighbour separation the concentration of

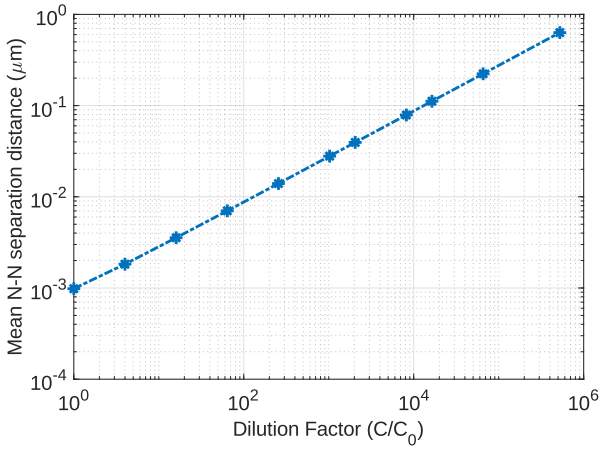

Figure 7: The plot shows the estimated mean nearest-neighbour (N-N) separation distance between donor-acceptor pairs as a function of acceptor density (dilution factor).

acceptor dye molecules is determined by Beer-Lambart law. R6G doped PMMA thinfilms are prepared on a glass substrate and the transmittance T through the films is measured. Then, the concentration of the dye molecules is estimated using

$$c = \frac{-logT}{L\sigma_A} \tag{6}$$

where L is the thickness of the R6G doped PMMA films and σ_A is the absorption cross-section of R6G. We estimate the acceptor dye molecule number density to be $\sim 3 \times 10^{24}$ molecules/m^3

Persistence of interactions

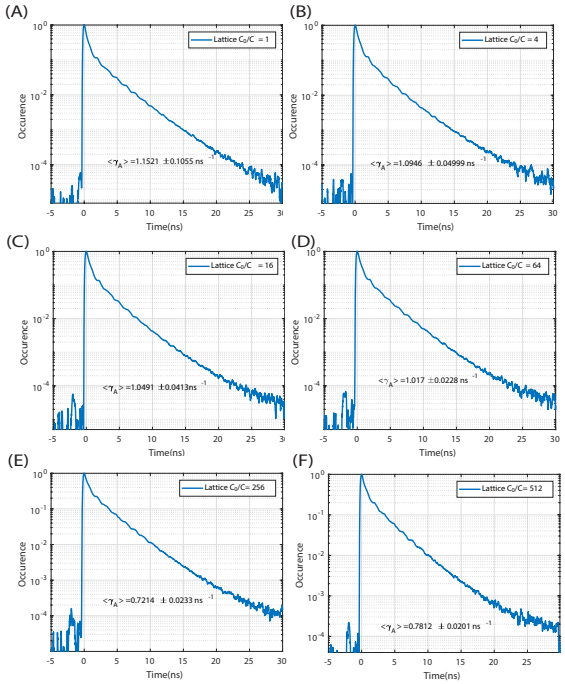

Figure 8: The plot shows the fluorescence decay lifetime of the acceptor molecules only on the plasmonic lattice at different dilution factors.

We also notice that the energy transfer efficiency remains $\sim>0.3$ up to $\sim$16384 dilution factor ($\sim$150 nm-200 nm mean N-N separation distance). This observation indicates that at large donor-acceptor mean nearest-neighbour separation distances statistically, $\sim 1/3$ of the donor molecules are interacting with the sparsely available acceptor molecules. This intriguing result can be understood from the mean decay lifetime of the donor only and acceptor only on the plasmonic lattice. The mean decay lifetime of the donors only on the plasmonic lattice is $\sim$9.7 ns while the mean decay lifetime of the acceptors is $\sim$0.87 ns, Fig. 8 ($\sim$2.6 ns on glass, see Fig. 9). The reduced lifetime is attributed to the increase LDOS

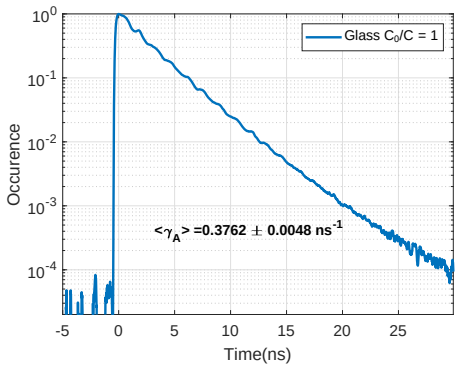

Figure 9: The plot shows fluorescence decay lifetime of acceptor molecules on glass. We note the lifetime to be ∼2.65 ns.

at acceptor's emission wavelength. Thus, in an ensemble of donors and acceptors, the same acceptor decays ∼11 times faster than the donor and as a consequence, an acceptor molecule that has decayed is available to interact with a different donor molecule within the same laser excitation cycle. This physically leads to more number of acceptor molecules being available for interaction with the donor molecules. within one excitation cycle. This increase in the number of available acceptor molecules leads to the statistical behaviour of ∼0.33 of the total donor molecules available for interaction with acceptor molecules. Furthermore, this experimental observation points towards the fact that in many-body DDI systems the LDOS at the acceptor emission wavelength also plays a crucial role in the strength and range of resonant energy transfer.

Mean decay rate statistics

At lower concentrations, the mean decay rates measured on the plasmonic lattice show a spread Fig. 10. This observation is indicative of the sensitivity of resonant energy transfer on availability of an acceptor molecule in the vicinity of a donor molecule. As the dilution factor increases, the mean separation between the donor-acceptor molecules increases. Thus, at large dilution factors the number of available acceptor molecules to the donor molecules within the laser excitation spot varies across different spots on the sample. This leads to

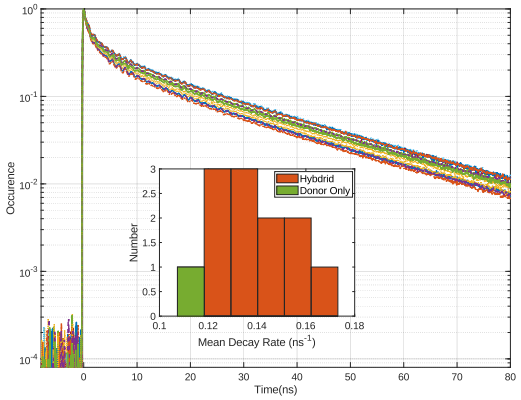

Figure 10: The plot shows the spread in lifetime decay trace at high concentrations ($C_0/C = 65536$). The inset shows in distribution of mean decay rates of donors in presence of acceptors (labelled as hybrid) in comparison to donors only on the plasmonic lattice.

large statistical spread in mean decay rate values and thus in the energy transfer efficiencies

References

(1) Lumerical Inc.

(2) Novotny, L.; Hecht, B. *Principles of nano-optics*; Cambridge University Press, 2012.

(3) Torquato, S.; Lu, B.; Rubinstein, J. Nearest-neighbour distribution function for systems on interacting particles. *Journal of Physics A: Mathematical and General* **1990**, *23*, L103.